Peer-reviewed version available at Energies 2019, 12, 1576; doi:10.3390/en12081576

Article

Modular Rotor Single Phase Field Excited Flux Switching Machine With Non-Overlapped Windings

Lutf Ur Rahman*, Faisal Khan , Areej Fatima, Muhammad Afzal Khan, Naseer Ahmad, Mohsin Shahzad, Hamid Ali Khan, Hazrat Ali

COMSATS University Islamabad, Abbottabad Campus, Pakistan.

lutfurrahman65@yahoo.com, faisalkhan@cuiatd.edu.pk, areejfatima94@hotmail.com, afzal.0370@gmail.com, n.ahmadmwt@gmail.com, mohsinshahzad@cuiatd.edu.pk, hamidalims@gmail.com, hazratali@cuiatd.edu.pk,
* Correspondence: lutfurrahman65@yahoo.com

Abstract: In recent years, numerous topologies of single phase and three phase Field Excited Flux-Switching Machine (FEFSM) have been developed for several applications. Comparative study of three types of single-phase low-priced Field Excited Flux-Switching Machine (FEFSM) is presented in this paper. Both the conventional 8S/4P sub-part rotor design and 6S/3P salient rotor design have an overlapped winding arrangements between armature coil and field excitation coil that depicts high copper losses as well as results in increased size of motor. Additionally, FEFSM with salient structure of the rotor have high flux strength in the stator-core that has much impact on high iron losses. Copper consumption and iron loss being a crucial proportion in total machine losses. Therefore a novel topology of single phase modular rotor field excited FSM with 8S/6P configuration is proposed, which enable non-overlap arrangement between armature coil and FEC winding that facilitates devaluation in the copper losses. The proposed modular rotor design acquires reduced iron losses as well as reduced active rotor mass comparatively to conventional rotor design. It is very persuasive to analyze the best range of speed for these rotors to avoid cracks and deformation, the maximum tensile strength (can be measured with principal stress in research) of the rotor analysis is conducted using JMAG. A deterministic optimization technique is used to enhance the performance of 8S/6P modular rotor design. The electromagnetic performance of conventional sub-part rotor design, F1-A3-3P design and proposed novel-modular rotor design are analyzed by 3D-Finite Element Analysis (3D-FEA), includes flux linkage, flux distribution, flux strength, back-EMF, cogging torque, torque characteristics, iron losses and efficiency.

Keywords: Flux switching machine, Modular rotor, non-overlap winding, magnetic flux analysis, iron losses, copper loss, stress analysis, Finite Element Method.

1. Introduction

In everyday application, universal motors are mostly used such as power tools, blenders and fans. They are operated at high speed and deliver high starting torque as getting direct power from ac-grid. At high speed, universal motor causes noise due to their mechanical commutators, and have comparatively short maintenance period. To cope with these snags, research of high performance and low-cost brushless machine is greatly in demand [1].

Switched-Flux brushless machines, a new class of electric machine that was first presented in 1950s [2]. Flux Switching Machines (FSMs), an unconventional machine originated from the combination of principles among induction alternator and switched reluctance motor [3]. A distinct feature of FSM has high torque density and robust structure of rotor by putting all excitation on stator. In the course of most recent decade various novel FSMs have been developed for several applications, confines from domestic appliances [4], automotive application, Electric vehicles [5], wind power and aerospace [6]. FSM is categorized into Permanent Magnet Flux Switching Machine (PMFSM), Field

Preprints (www.preprints.org) | NOT PEER-REVIEWED | Posted: 18 December 2018 doi:10.20944/preprints201812.0208.v1

Peer-reviewed version available at Energies 2019, 12, 1576; doi:10.3390/en12081576

Excited Flux Switching Machine (FEFSM), and Hybrid Excited Flux Switching Machine (HEFSM). Permanent magnet FSM and Field Excited FSM has permanent magnet (PM) and field excitation coil (FEC) for generation of flux source respectively, whilst both PM and FEC are generation sources of flux in HEFSM. The major advantage of FSM has simple/robust structure of rotor and easy management of temperature rise as all the excitation housed on stator. Recently, use of permanent magnet as a primary source of excitation has dominated in flux switching research, due to its high torque/ high power density and optimum efficiency [7]. However, the maximum working temperature of PM is limited due to potential irreversible demagnetization. The use of PM in not always desirable due to high cost of rare earth material. For low cost applications, it is desirable to reduce the use of permanent magnet and hence is replace by DC-FEC. FEFSM has capable of strengthening and weakening the generated flux as it is controlled by DC-current. FEFSM has disadvantage of less starting torque, fixed rotational direction and high copper losses. The cumulative advantages of both FEC and PM are embedded in HEFSM having high torque capability/high torque density, HEFSM also have high efficiency and flux weakening capability. However, the demerits of HEFSM include more complex structure, saturation of stator-core due to use of PM on stator, greater axial length and having high cost because of rare earth material. Therefore, FEFSM could be considered as better alternative for requirement of low cost, wide speed controllability, high torque density, simple construction, permanent magnet less, and flux weakening operations as compared to other FSMs.

Numerous single-phase novel FS machines topologies has been developed for household appliances and different electric means. Single phase FSM was first presented in [8] and further investigated in [9] [10] by C. Pollock, it has 8S-4P doubly salient machine that offers high power density and low cost as shown in Figure 1. The FEC and armature has an overlapped winding arrangements resulting in longer end winding. To overcome the drawback of long end winding, 12S-6P FSM has been developed that has same coil pitch as 8 stator slots and 4 rotor poles but shorter end winding [11]. Figure 2. depicts that 12-slots/6-poles machine have fully pitched winding arrangement as C. Pollock design. The end windings effect has even shorter by re-arranging the armature winding and FEC to different pitch of 1 and 3 slot pitches as shown in Figure 3. Both machine having F2-A2-6-pole and F1-A3-6-pole coil pitches have better copper consumption then conventional machine(F2-A2 4pole) for short axial length but has a disadvantage of higher iron loss due to more rotor poles [12]. The stator slots and rotor poles could be halved into F1-A3-3P machine as shown in Figure 4. , that is much appropriate for high speed because of significant reduction in iron loss. When the axial length is short that is up to 25 mm the average torque of both F2-A2/4P and 6-Pole machine is similar. However, F1-A3/3P exhibit higher average torque than F1-A3/6P machine at longer axial length of 60 mm. At the point when end winding is disregarded, the machine having more stator teeth's and rotor poles has less average torque as compared to machine having less rotor poles and slots of stator for same type of machine.

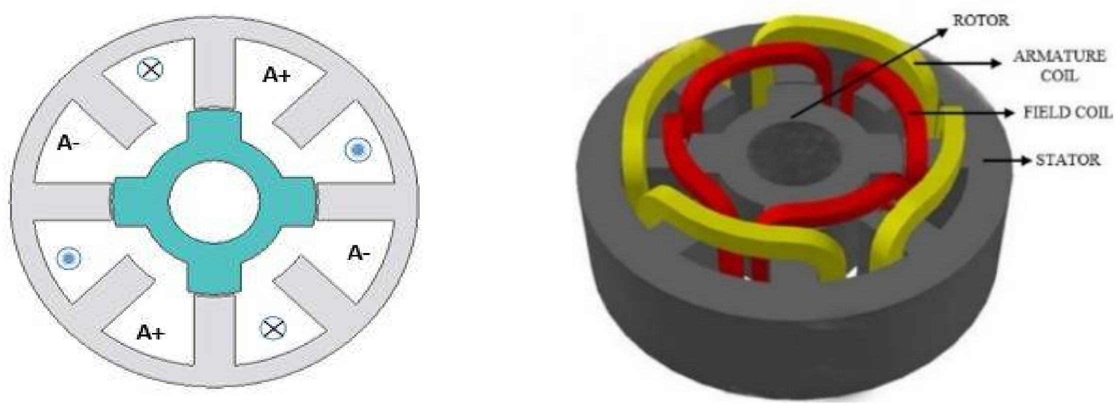

(a) (b)

Figure 1. 8S/4P FEFS machine (F2-A2-4P). (a) cross sectional (b) 3D-model[11]

 doi:10.20944/preprints201812.0208.v1

Peer-reviewed version available at *Energies* **2019**, *12*, 1576; doi:10.3390/en12081576

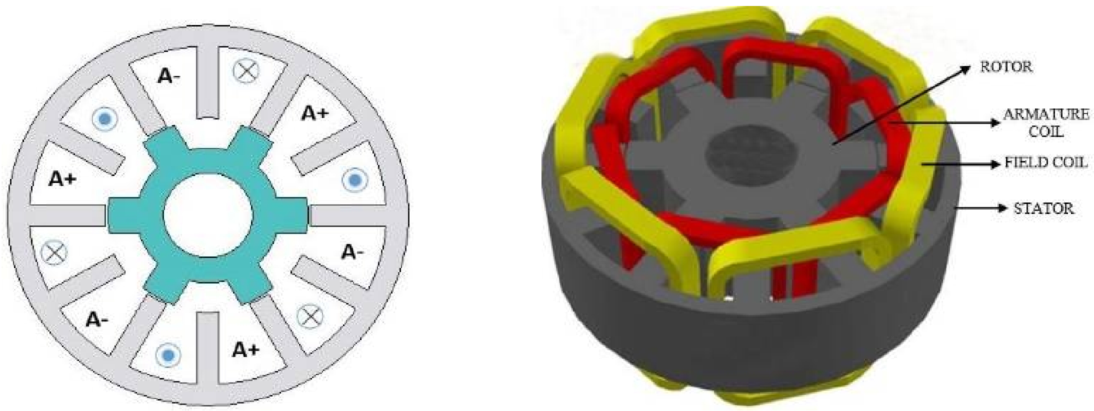

(**a**) (**b**)

Figure 2. 12S/6P FEFS machine (F2-A2-6P) . (a) cross sectional (b) 3D-model[11]

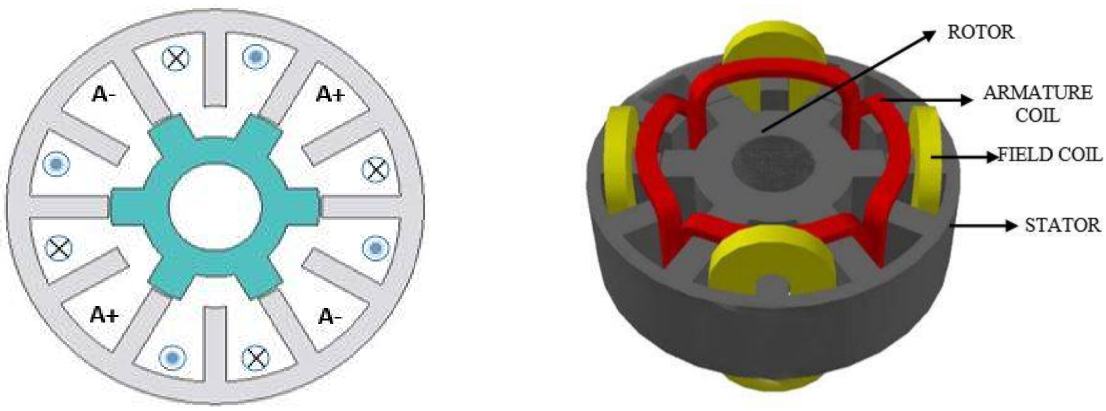

(**a**) (**b**)

Figure 3. 12S/6P FEFS machine with rearranged winding (F1-A3-6P) . (a) cross sectional (b) 3D-model[11]

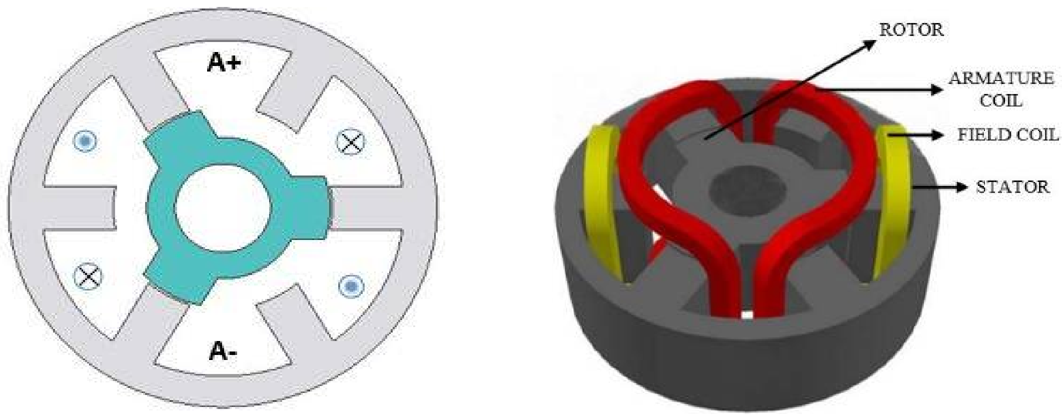

(**a**) (**b**)

Figure 4. 6S/3P FEFS machine (F1-A3-6P) . (a) cross sectional (b) 3D-model[11]

In single phase FS machine torque is generated with doubly salient structure due to the tendency of rotor to align itself into a minimum reluctance position as shown in Figure 5. When the stator slot and rotor pole is aligned at a minimum reluctance position, the motor couldn't generate torque (called dead zone torque) at aligned positions unless armature current direction is reversed. Dead zone of torque is eliminated in [13] with sub-part rotor structure having different pole arc lengths. The 8-slots/4-poles sub-part rotors are merged on same face and the pole axes are not parallel. However, sub-rotor poles can't be allied with stator slots at a same-time, thus reluctance torque is generated at any rotor position. The single phase 8S/4P sub-part rotor FSM only applicable for a situation that requires a continuous unidirectional rotation. The conventional sub-part rotor design has demerit of overlapped winding arrangements between FEC and armature winding that result in higher copper consumption, and higher iron losses due to salient rotor structure. Single phase sub-rotor FS machine minimize the advantage of high speed, it cannot operate at speed higher than normal level.

This paper presents a novel-modular rotor structure for single phase FS machine as shown in Fig 6. The proposed design comprises of non-overlapped winding arrangements between armature winding and FEC, and modular rotor structure. The consumption of copper is much reduced due to non-overlapped winding arrangements. The modular rotor single phase FSM exhibit a significant reduction in iron losses, also reduces the rotor mass and lower the use of stator back-iron without diminishing in output torque.

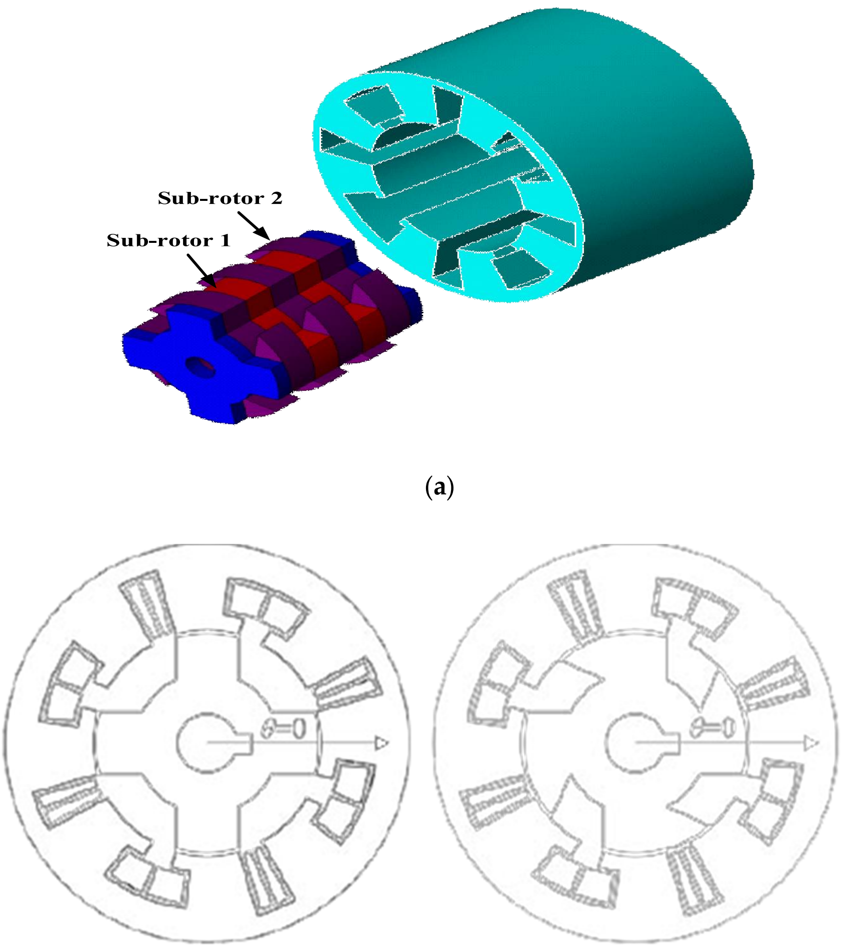

(b) (c)

Figure 5. Sub-part rotor structure (a) manifestation of sub-part rotor (b) pole arc of sub rotor-1 (c) pole arc of sub rotor-2.

Preprints (www.preprints.org) | NOT PEER-REVIEWED | Posted: 18 December 2018 doi:10.20944/preprints201812.0208.v1

Peer-reviewed version available at *Energies* **2019**, *12*, 1576; doi:10.3390/en12081576

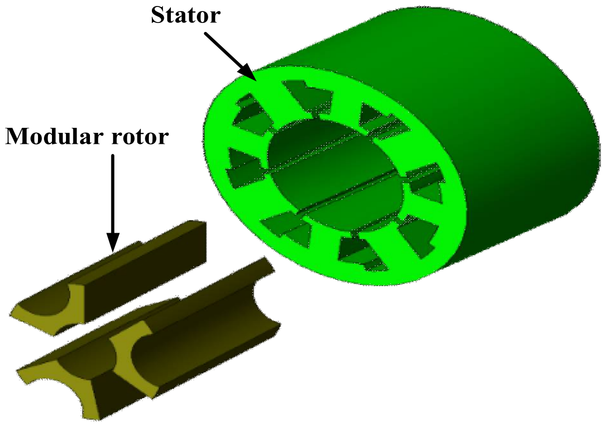

Figure 6. Modular rotor structure.

2. Design Methodology

The proposed novel modular rotor single phase 8-slots/6-poles FEFSM with non-overlap winding arrangements is presented, as shown in Figure 7. To design the modular structure, JMAG designer ver.14.1 is used and the results obtained are validated by the 3D Finite Element Analysis (3D-FEA). First of all, every section of motor such as stator, rotor, field excitation coil (FEC) and armature coil of modular design with 8-stator slots and 6 rotor poles is designed in the Geometry Editor. Then, the material, mesh properties, circuit, various properties and conditions of the machine is selected and simulated in the JMAG designer. The stainless steel sheet of soft magnetic material 35A210, is used for stator and rotor core. The design parameters and specifications of the modular design is illustrated in Table 1.

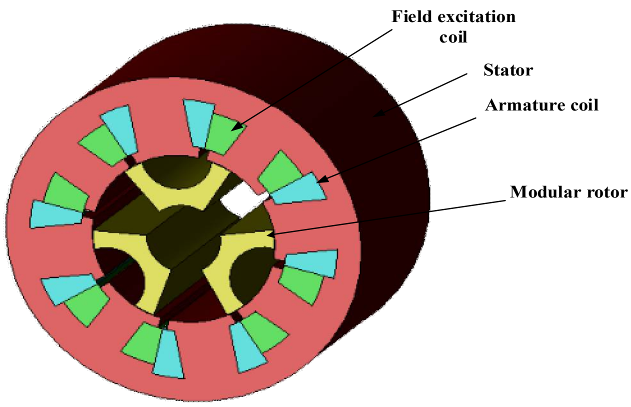

Figure 7. 8S-6P FEFSM with Modular rotor

3. Deterministic Optimization

The average torque analyses of 8-stator slots/6-rotor poles are examined. The maximum output torque obtained by the initial design is 0.88Nm at speed of 400rpm, which is much lower from the other designs. In order to improve the average torque characteristics, deterministic optimization is used. Design free parameters RIR, θ, SR, TWA, TRA, TWD and TRD are defined in rotor and stator part, as depicts in Figure 8 are optimized, while the outer radius of stator, air gap and shaft of the motor are kept constant. First optimization cycle consists of five steps, that is RIR, θ, SR, TWA, TRA, TWD and TRD.

Peer-reviewed version available at Energies 2019, 12, 1576; doi:10.3390/en12081576

TABLE 1. Design parameter of machines

Design Parameters	F1-A3-3P	Sub-part rotor design	Modular rotor design
Number of phase	1	1	1
No. of slots	6	8	8
No. of pole	3	4	6
Stator outer diameter	96 mm	96 mm	96 mm
Rotor outer diameter	55.35mm	53.55 mm	53.55 mm
Air-gap	0.45	0.45 mm	0.45 mm
Rotor inner diameter	21 mm	10 mm	20 mm
Stator pole arc length	-	15.2 mm	5.5 mm
Teeth's arc of sub-rotor-1	-	15.2 mm	-
Teeth's arc of sub-rotor-2	-	26.9 mm	-
Rotor pole width	8 mm	-	5.6 mm
Stack length	60 mm	60 mm	60 mm
No. of turns per phase	120	30	30

Initially, the design free parameters of rotor is updated, first of all, the inner rotor radius, RIR, are change while the keeping other parameters of stator and rotor are constant. Then, rotor pole angle, θ, and split ratio Ss, are varied and adjusted. The rotor pole angle, θ, is a dominant parameter in modular design to increase torque characteristics. Once the combination of promising values of rotor part for highest average output torque is determined, the next step is to refine the TWD and TRD of FEC, while rotor and armature slot parameter are kept constant. Finally, the essential armature slot is optimized by changing TWA and TRA while all other design parameters are preserved. To attain the highest average output torque, the above design optimization process is repeated. Figure 9. illustrates the highest average torque result after two cycles of optimization by updating several parameters that is already mentioned above. From Figure 9, it is also clear that during the first cycle the torque increases to a certain level by varying above parameters of machine and formerly becomes constant.

During the first cycle, 32 percent of increase in the average output torque is achieved by refining the dominant parameter of rotor pole angle, θ, whilst other free design parameter adjustment show a less improvement in torque. In comparison with the initial design the average output torque is improved by 40 percent after completion of second optimization cycle. The initial and optimized structure of 8S/6P modular design is illustrated in Figure 10. Additionally, the comparison of parameters of initial and final design is presented in Table 2.

Table 3. depicts comparison of cogging torque, flux linkage, back-EMF, average torque, and power of 3D-modular un-optimized and optimized design. The cogging torque and flux linkage of optimized designs is 0.3374Nm and 0.2114Wb respectively, which is 50% lower than the un-optimized cogging torque and flux linkage. Whilst, back-EMF of optimized modular 8S/4P is improved by 15%, that is still much lower than the applied input voltage of 220V. Furthermore, before optimization of modular design the maximum average output torque and power obtained is 9.77Nm and 162.9Watts respectively, at maximum FEC current density, Je, is set to 10A/mm2 and 25A/mm2 is assigned to the armature coil, which is improved to 1.66Nm and 288Watts, respectively. Comparatively, average output torque and power is improved by 58.85% and 56.40%, respectively.

Preprints (www.preprints.org) | NOT PEER-REVIEWED | Posted: 18 December 2018 doi:10.20944/preprints201812.0208.v1

Peer-reviewed version available at *Energies* **2019**, *12*, 1576; doi:10.3390/en12081576

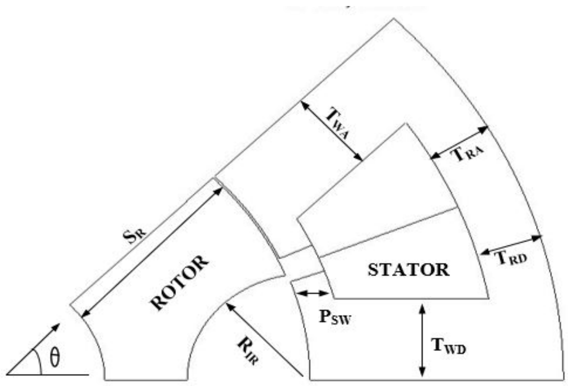

Figure 8. Design parameters of modular rotor design.

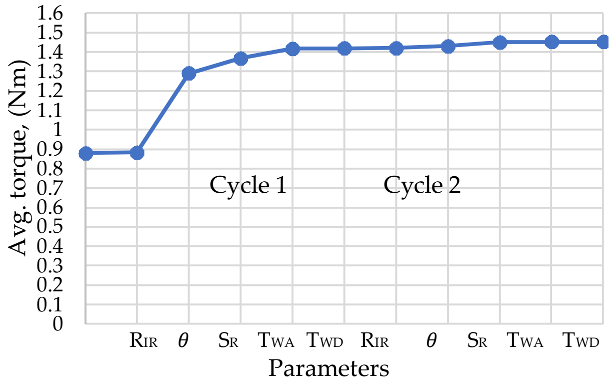

Figure 9. Effect of design parameters on average torque

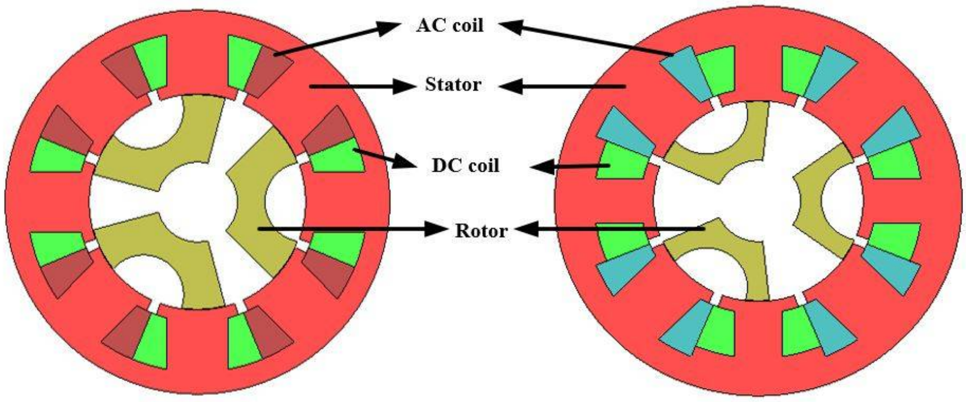

(**a**) (**b**)

Figure 10. Structure of 8-slots/6-poles modular design.

Table 2. Initial and refined design parameters of Novel-modular rotor design

Parameters	Units	Initial values	optimized values
Outer stator (OS)	mm	48	48
Inner stator (IS)	mm	27	24.7
Back-iron width of AC (T_{RA})	mm	42.5	41.4
Tooth width of AC (T_{WA})	mm	7.6	7.5
Back-iron width of DC (T_{RA})	mm	42.5	38.66
Tooth width of DC (T_{WD})	mm	7.6	5.5
Rotor inner circle radius (R_{IR})	mm	10	9.7
Pole shoe width (P_{SW})	mm	3	3
Rotor pole angle (θ)	deg	45	36
Split ratio (S_R)	-	0.55	0.5
Air gap	mm	0.45	0.45
Shaft radius	mm	10	10
Avg. torque	Nm	0.880	1.454

Preprints (www.preprints.org) | NOT PEER-REVIEWED | Posted: 18 December 2018 doi:10.20944/preprints201812.0208.v1

Peer-reviewed version available at Energies 2019, 12, 1576; doi:10.3390/en12081576

Table 3. Results comparison of optimized and un-optimized design

--	Cogging torque (Nm)	Flux linkage (Wb)	Back-EMF (volt)	Avg. Torque (Nm)	Power (Watts)
Un-optimized design	0.67	0.01060	3.9	0.97775	162.986
Optimized design	0.3374	0.02114	4.6	1.66148	288.967

4. Result And Performance Based On 3D-FEA Finite Element Analysis (3D-FEA)

4.1. Flux Linkage

Comparison of flux linkages of three field excited FSM at no-load is validated by 3D-FEA. To analyze the sinusoidal behavior of flux, the input current density of FEC and armature coil is fixed to 10 A/mm² and 0 A/mm² respectively. Figure 11. shows that proposed modular design has peak flux of 0.021Wb which is approximately equal to the peak flux of 15% of F1-A3-3P design. Similarly, sub-part rotor design has 66% higher peak flux linkage than 8S/6P modular structure due to different pole arc length. The conventional F1-A3-3P design has highest peak flux as compared to modular design as well as sub-part rotor design due to the doubly salient structure.

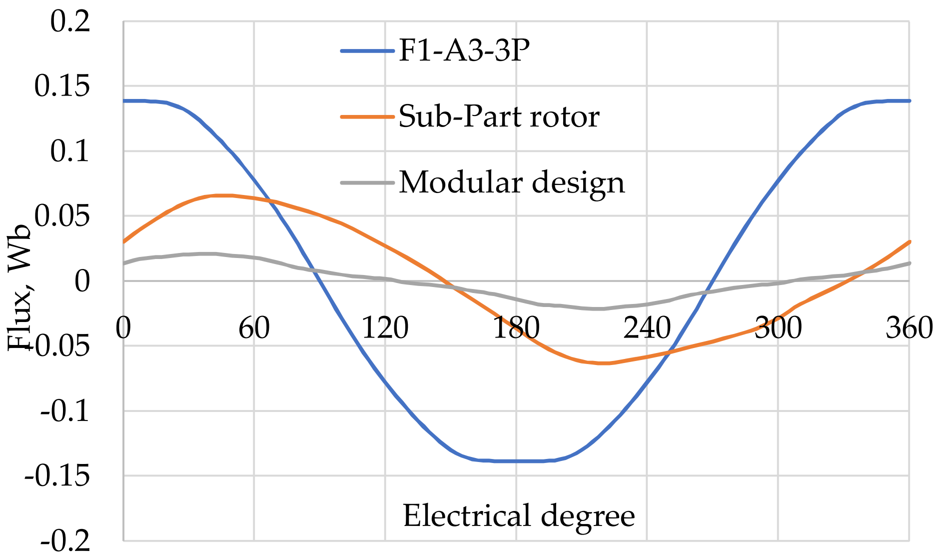

Figure 11. Comparison of U-flux linkages.

4.2. Flux Distribution

Flux density distribution generated by the DC coil in three FEFSM is shown in Figure 12. The red spot mention in Figure 12 (a) and (c) show saturation of stator teeth and back-iron respectively of both conventional designs. F1-A3-3P design and sub-part rotor design has vector plot value of magnetic flux density distribution of 1.9953 and 1.9760 maximum, respectively. Whilst, the flux density distribution of modular design from the vector plot is 2.2528 maximum at 0° rotor position. Additionally, in comparison with 8S/4P sub-part rotor design and 6S/3P design, the proposed 8S/6P modular rotor design exhibits higher flux distribution. For completely utilizing flux in the proposed design, various parameters of machine is optimized to enhance the flux distribution from stator to rotor and vice versa.

 doi:10.20944/preprints201812.0208.v1

Peer-reviewed version available at *Energies* **2019**, *12*, 1576; doi:10.3390/en12081576

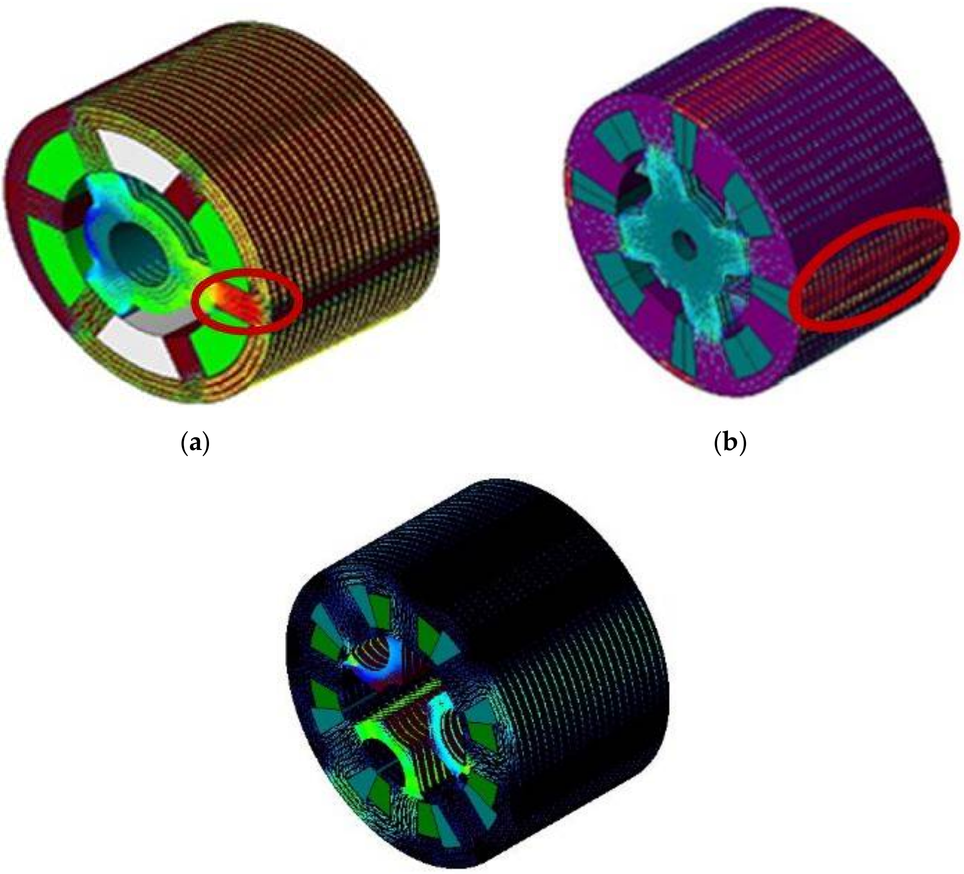

(**a**) (**b**)

(**c**)

Figure 12. Flux Distribution (a) Flux distribution conventional in F1-A3-3P design (b) Flux distribution in sub-part rotor design (c) Flux distribution in proposed modular rotor design

4.3. Flux Strengthening

The effect of flux strength is analyzed by increasing current density; J_e of field excitation coil (FEC) is varied from 0 A/mm² to 20 A/mm², whilst armature current density; J_a is set 0 A/mm². The FEC input current is calculated from "(1)".

$$I_e = \frac{J_e \alpha S_e}{N_e} \qquad (1)$$

Where, I_e, J_e, α, S_e and N_e are the input current of FEC, field current density, filling factor, slot area of FEC, and number of turns of field coil respectively. The analysis of coil test can be verified from the flux strengthening. With increasing the current densities of FEC the pattern plot clearly shows a linear increase in flux until 0.027 Wb at J_e of 20 A/mm² as shown in Figure 13.

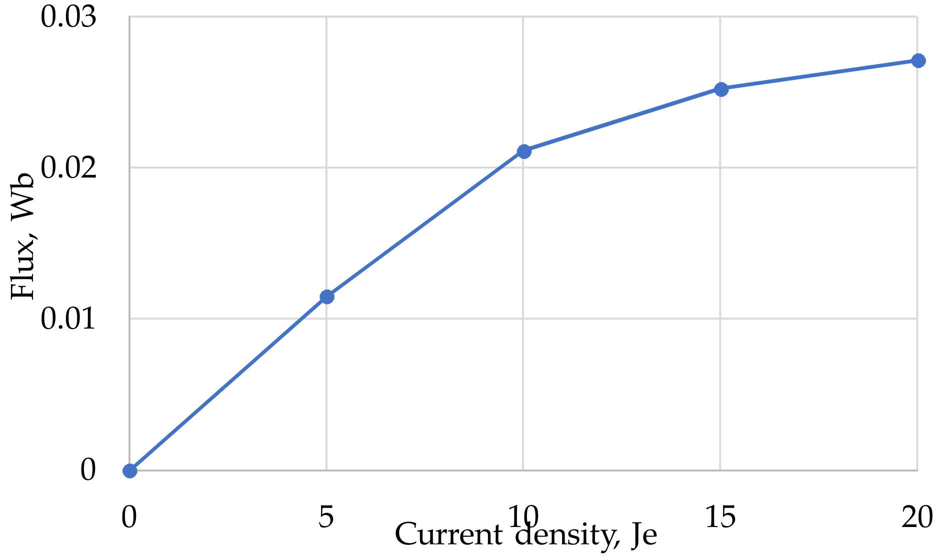

Figure 13. Peak flux strengthening with Modular rotor at various Je

4.4. Back-EMF Versus Speed

"Back-EMF is the induce voltages in the armature winding which opposes the change in current through which it is induced". The back-EMF (e_a) in the armature can be determined from the rate of change in armature flux or applying the co-energy concept [14]. For motor with N_r rotor poles

$$e_a = \omega\phi_f \frac{2KN_aN_r}{\pi} \tag{2}$$

Where N_a, N_r, ω, ϕ_f, and K is number of armature turns, number of rotor poles, rotational speed, field flux and constant of field flux that linking with armature winding respectively. Substituting the ϕ_f (field flux) with

$$\phi_f = \frac{N_fI_f}{\mathcal{R}} \tag{3}$$

$$e_a = \frac{2KN_r}{\pi\mathcal{R}} N_aN_fI_f\omega \tag{4}$$

Where N_f, I_f and $\mathcal{R}$ is the number of field turns, the field current and reluctance of magnetic circuit. For the maximum conversion of electro-mechanical energy, armature current must flow in opposite direction to the induced-EMF in armature.

Figure 14. shows the 3D-FEA predicted induced-EMF of 8-slots/6-poles modular rotor structure at a fixed field current density (Je; 10A/mm^2) and various speed. The induced-EMF is increases linearly with increasing speed. The maximum induced voltage is 22V at a maximum speed of 1600rpm which is quiet lower than the applied input voltage (220V) which confirm the motor actioning of machine.

Preprints (www.preprints.org) | NOT PEER-REVIEWED | Posted: 18 December 2018 doi:10.20944/preprints201812.0208.v1

Peer-reviewed version available at *Energies* **2019**, *12*, 1576; doi:10.3390/en12081576

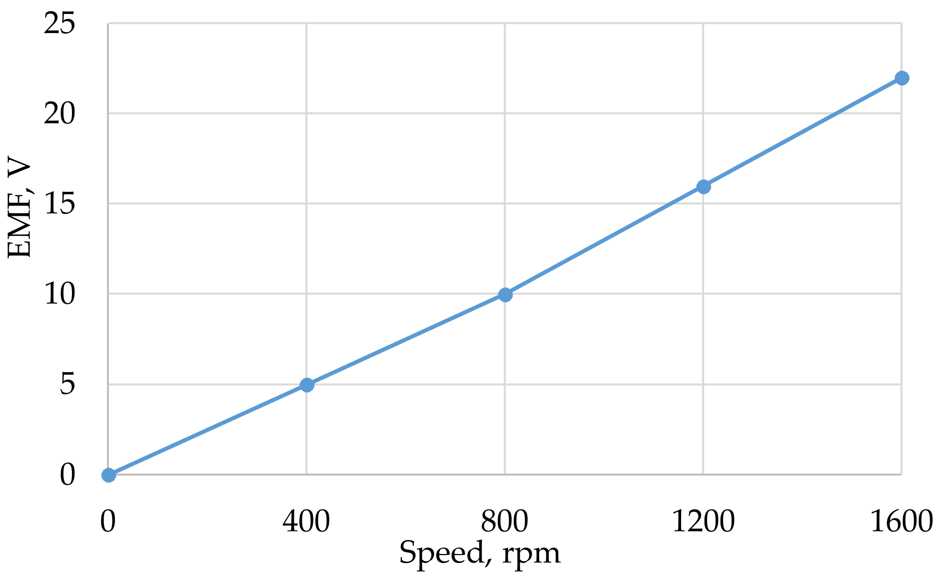

Figure 14. Maximum back-EMF at various speed

4.5. Total Harmonic Distortion(THD)

Total harmonics distortion is the ratio of the summation of all harmonic components to the fundamental frequency harmonics of the power or can say harmonics distortion that exists in signal. In electric machines, THD occurs due to harmonics present in flux. THD determines the electromagnetic performance of the machine as it is the representation of the harmonics in the machine. Mathematically THD of electric machine can derived from equation (5)

$$THD = \frac{\sqrt{\sum_{n=1,2\ldots}^{k=2n+1} \Phi_k^2}}{\Phi_1} \tag{5}$$

Where k is odd number and Φ_k is the odd harmonics of flux. THD of proposed design is higher as compare to conventional design due to the modular structure of rotor. Figure 15 shows the THD of three FEFS machine. The graph shows that the THD of sub-part rotor design and F1-A3-3P design is 7% and 4% respectively, while THD of proposed modular rotor design is 16.4%.

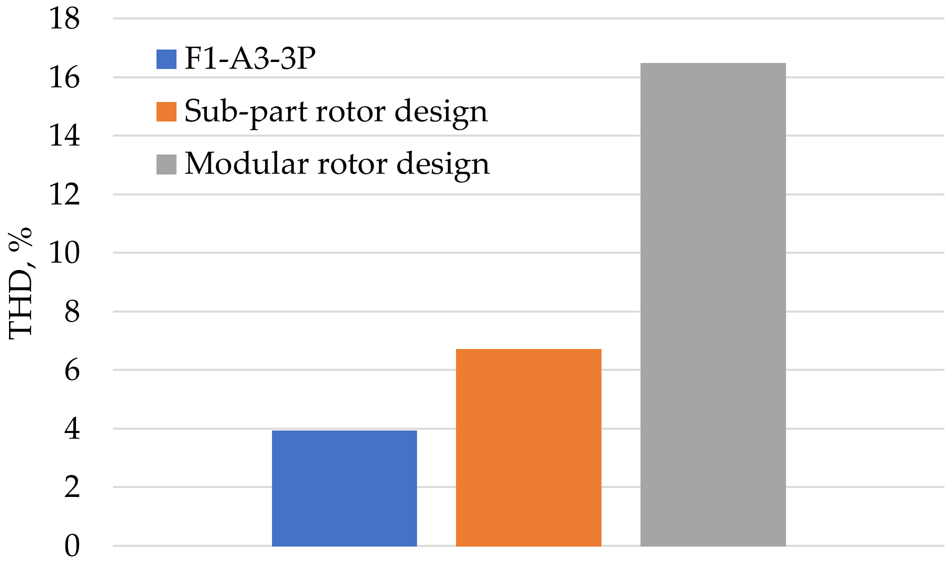

Figure 15. THD values of conventional and proposed design.

4.6. Cogging Torque

The interaction between the Stator excitation source (PM, excitation coil) and rotor pole of machine at no-load is called cogging torque. Magnetic circuit consists of an existing PM and coil having co-energy, the total co-energy is formulated as [15-16].

$$W_c = Ni\varphi_m + \frac{1}{2}(Li^2 + (\mathcal{R} + \mathcal{R}_m)\varphi_m{}^2) \tag{6}$$

Where, N, i, $\mathcal{R}_m$, L, $\mathcal{R}$ and φ_m are the number of turn, current, magnetic field, inductance of coil, magneto-motive force and magnetic flux linkage respectively. The change in total co-energy with respect mechanical angle of rotor determine the average torque of the machine.

$$T_e = \frac{\partial W_c}{\partial \theta} with\, i = constant \tag{7}$$

Where, W_c and θ are total co-energy and mechanical rotor angle and respectively.

$$T_e = \frac{\partial(Ni\varphi_m + \frac{1}{2}(Li^2 + (\mathcal{R} + \mathcal{R}_m)\varphi_m{}^2))}{\partial \theta}$$

$$T_e = Ni\frac{d\varphi_m}{d\theta} + \frac{1}{2}i^2\frac{dL}{d\theta} - \frac{1}{2}\varphi_m{}^2\frac{d\mathcal{R}}{d\theta} \tag{8}$$

The 3rd term in eq. (8) change in mmf w. r. t mechanical position of rotor causes cogging torque. The cogging torque produces unwanted noise and vibration. As the eq (8) shows that the cogging torque lead to a significant reduction in the average torque.

The cogging torque of F1-A3-3P, Sub- part rotor and modular designs is compare in Figure 16. The cogging of Modular design is less than F1-A3-3P and Sub- part rotor designs as depicts in Figure 16. Figure 16. Illustrates that the cogging torque of modular design is 12% of F1-A3-3P and 53% of Sub- part rotator. As a result the modular design has less vibration and more average torque as to compare to F1-A3-3P and Sub-part rotator design.

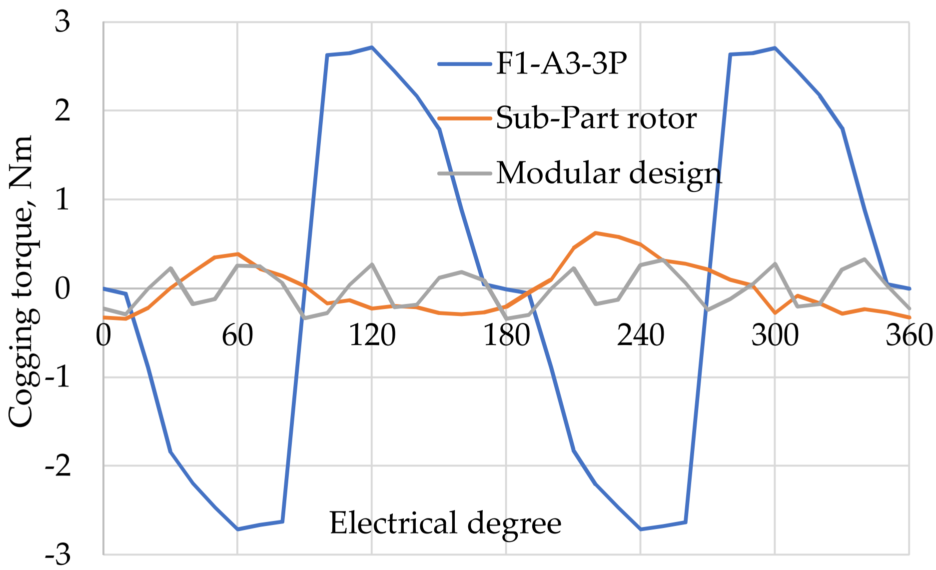

Figure. 16 Comparison of Cogging torque

4.7. Copper Loss Vs Torque

In field excited FSM, the copper consumption is the main constituent affecting the overall cost of the machine. As compare to other material of FEFSM copper is more expensive. The copper-loss of single phase FEFSM can be calculated from the formula as;

$$P_{Cu} = I_a^2 R_a + I_f^2 R_f \tag{9}$$

Where I_a, R_a, I_f, R_f is the armature current, armature winding resistance, field current, field winding resistance respectively. The comparison of copper loss-torque curve of three field excited FSM is shown in Figure 17. The average output torque modular design is almost similar to the sub-part rotor design but is much higher than the F1-A3-3P design. At fixed copper loss of 60 watt the average torque of conventional sub-part rotor design, F1-A3-3P design and proposed modular design is 1.6 N-m, 0.98 N-m and 1.58 N-m respectively. However, the plot clearly shows that modular design achieve higher average torque under constraint of maximum copper loss of 120 watt due to the short pitch coils.

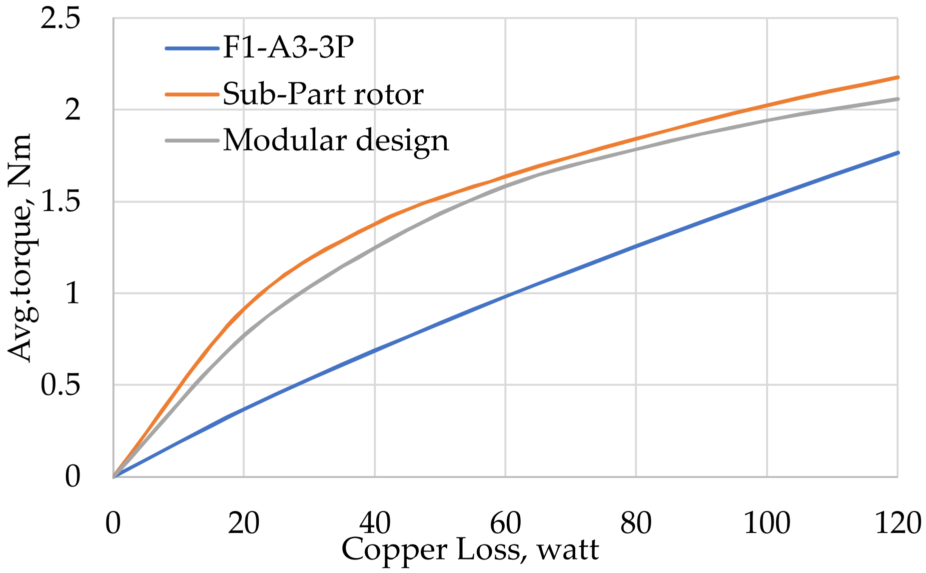

Figure. 17 Comparison of average torque at fixed copper losses.

4.8. Torque Density And Power Density

Torque density and power density of three FEFS machine is calculated at fixed current density of $10A/mm^2$. Figure 18. illustrates torque densities of sub-part rotor design, F1-A3-3P design and modular rotor design. Comparatively, torque density of F1-A3-3P design is 1.89 times higher than modular rotor design and 1.71 times higher than sub-part rotor design as shown in Figure 18.

The power density of conventional and proposed design is expressed in Figure 19. Power density attains by modular rotor design is 0.0783Watt/kg at current density of FEC,J_E, and armature current density, J_A, of $10A/mm^2$ as shown in Figure 19. High power density exhibits high efficiency and better electromagnetic performance. The proposed 8S/4P modular rotor design achieve 1.3 and 1.9 times higher power densities as compared to F1-A3-3P design and sub-part rotor design respectively.

Preprints (www.preprints.org) | NOT PEER-REVIEWED | Posted: 18 December 2018 doi:10.20944/preprints201812.0208.v1

Peer-reviewed version available at Energies 2019, 12, 1576; doi:10.3390/en12081576

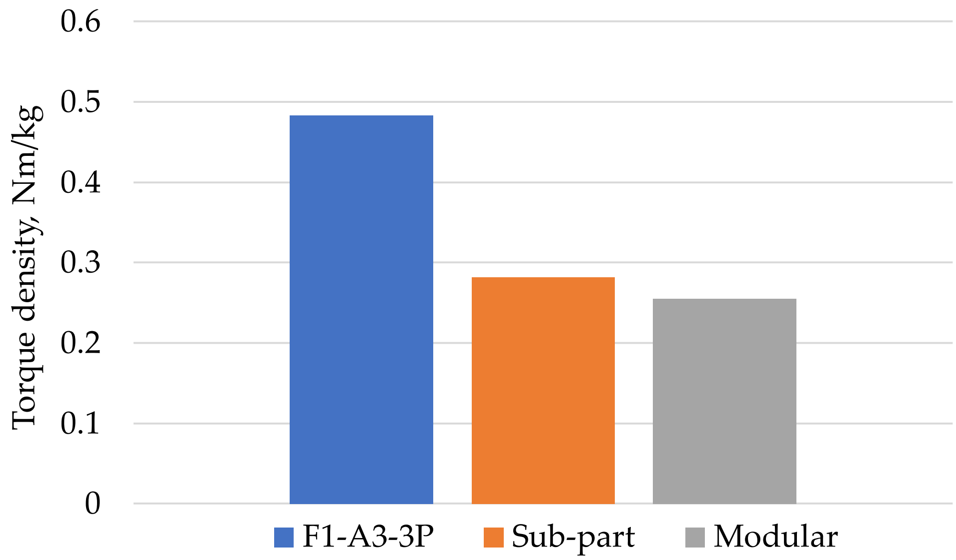

Figure 18. Torque density of three FEFS machines

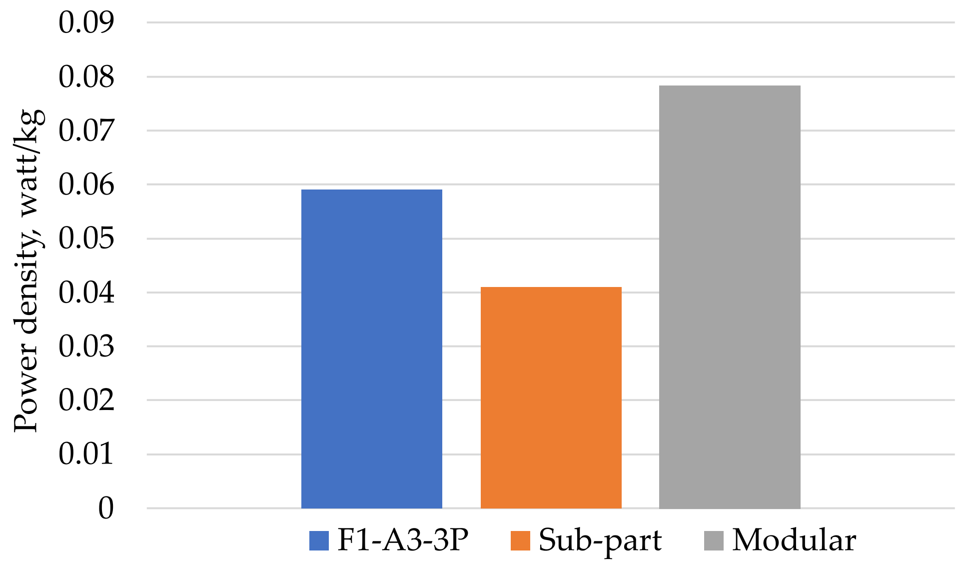

Figure 19. Power density of three FEFS machines

4.9. Torque And Power Versus Speed Characteristics

The comparison of torque and power versus speed curve of three single phase FEFSM are illustrated in Figure 20. At rated speed of 1664rpm, the maximum average torque of modular rotor design is 1.64Nm which correspond to the power generated by the proposed design is 286W. Additionally, the average torque obtained by conventional 8S-4P sub part rotor design and 6S-3P salient rotor is 1.4Nm and 3.77Nm, at a base speed of 1389rpm and 1053rpm, respectively. The average torque of proposed design is higher as compared to the sub part rotor design. At speed of 1600rpm, the average torque of proposed design is similar to 6S-3P design while 19 percent higher than 8S-4P design. Although, the generated power of 8S-6P modular design is 28.4 percent higher than 8S-4P design, while 31 percent lower than F1-A3-3P design. The pattern plot shows that beyond rated speed average torque of the machine starts to decrease and power is decreased as well. The power of 6S-3P FEFSM decreases more rapidly due to increase in iron loss above the rated speed.

Preprints (www.preprints.org) | NOT PEER-REVIEWED | Posted: 18 December 2018 doi:10.20944/preprints201812.0208.v1

Peer-reviewed version available at *Energies* **2019**, *12*, 1576; doi:10.3390/en12081576

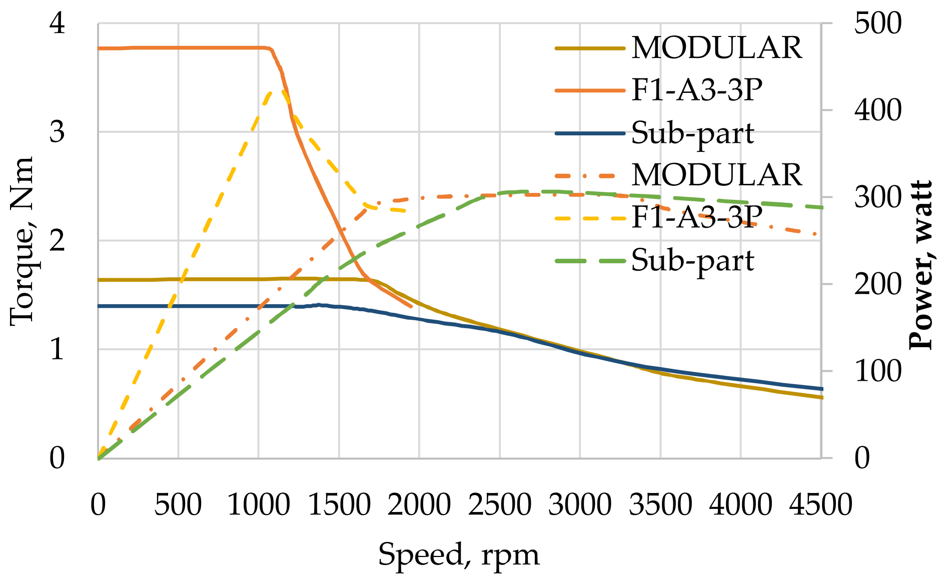

Figure 20. Comparison of torque/power versus speed of three FEFSM. (The dotted lines in the plot shows the power curve, while solid line depicts the torque curve at various speed)

4.10. Rotor Stress Versus Speed

Rotor stress analysis is a technique to identify the principal stress, nodal force and displacement occurred in the rotor structure in an ideal state after load is applied. Generally, condition for mechanical stress of the rotor structure is accomplished by centrifugal force due to the longitudinal rotation of rotor. Additionally, centrifugal force of the rotor is greatly affected with the speed. Rotor could highly withstand to the stress, if the principal stress of the rotor is higher. Principal stress is a crucial result in the analysis of stress. With increasing the angular velocity of the rotor principal stress is increased exponentially. Thus, the rotor principal stress verses speed of the three field excited flux switching machines (rotor structure) is analyzed using 3D-FEA. The angular velocity varies from 0rpm to 20000rpm for conventional three pole salient rotor structure, four pole sub-part rotor structure and proposed 6 poles modular structure to analyze the maximum capability of mechanical stress. The constraints that coincide to the force acting on the rotor is faces, edges and vertices. Positions of the constraints for each rotor structure are different as shown in Figure 21, 22, and 23.

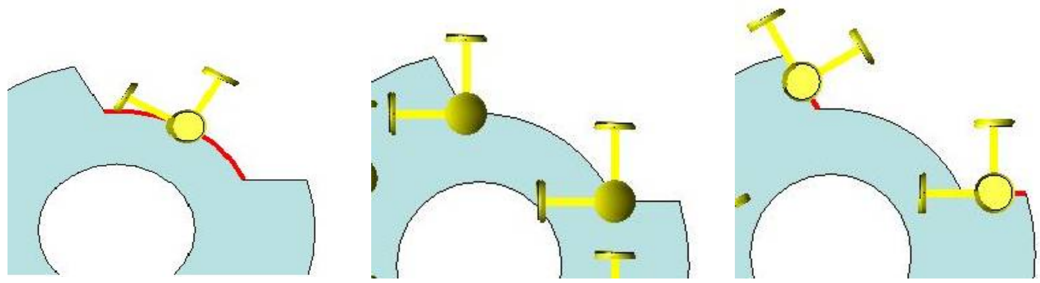

(a) (b) (c)

Figure.21 Direction of constraints for salient rotor structure

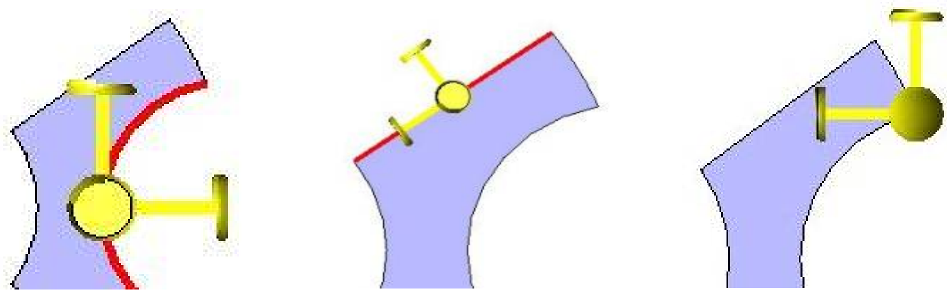

(a) (b) (c)

Figure. 22 Direction of constraints for modular rotor structure

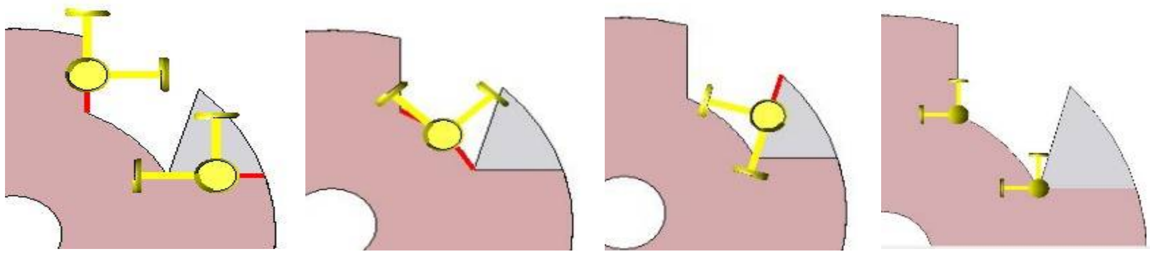

(a) (b) (c) (d)

Figure 23. Direction of constraints for sub-part rotor structure.

Figure 24 shows that comparison of principal stress of three different rotor structures versus speed. At maximum speed of 20000rpm, the principal stress of salient rotor structure, sub-part rotor structure and modular rotor structure is 6.73MPa, 11.61MPa and 2.11MPa respectively. The pattern plot clearly shows that principal stress of proposed modular rotor structure is much lower as compared to the conventional rotor design. The maximum allowable principal stress of 35H210 electromagnetic steel is 300MPa. All the three rotor structures are capable for high speed application, but only salient rotor structure can be operated at high speed due to the single piece rotor structure. Whilst, sub-part rotor and modular structure is only applicable for low-speed applications.

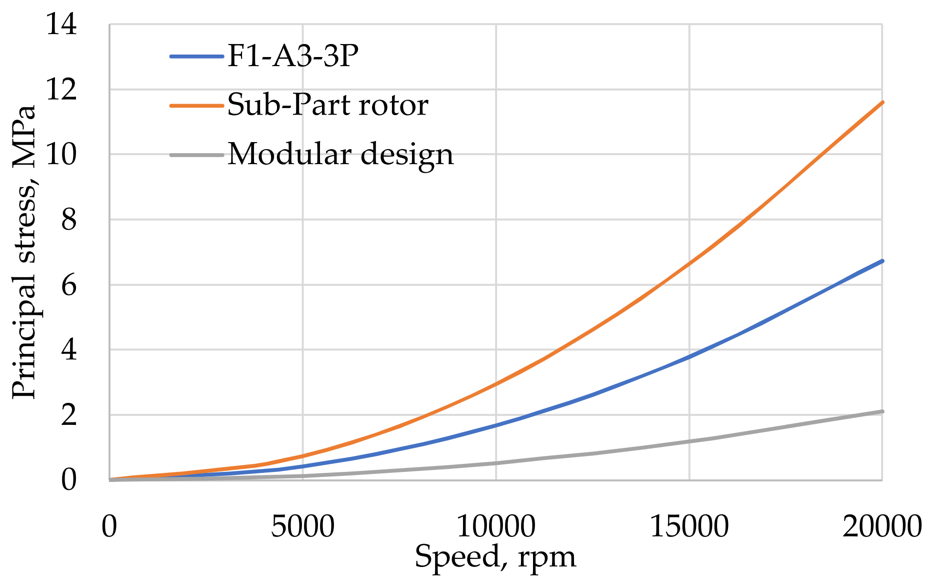

Figure 24. Principal Stress against speed

4.11. Copper Losses Versus J_E At Various J_A

Copper losses of three FEFSM at various armature current densities is shown in Figure 25. To analyze the total copper losses, FEC current density, J_E, is set to 10A/mm², and armature current density is varied from 0A/mm² to 25A/mm². The pattern plot clearly showed that the copper losses is increased with increasing current densities. Comparatively, proposed modular rotor design shows approximately 56% and 88% lower copper losses to sub-part rotor design and F1-A3-3P design respectively, at maximum armature current density of 25A/mm². However, the proposed structure has reduced copper losses indicating improved efficiency than the conventional designs.

Peer-reviewed version available at Energies 2019, 12, 1576; doi:10.3390/en12081576

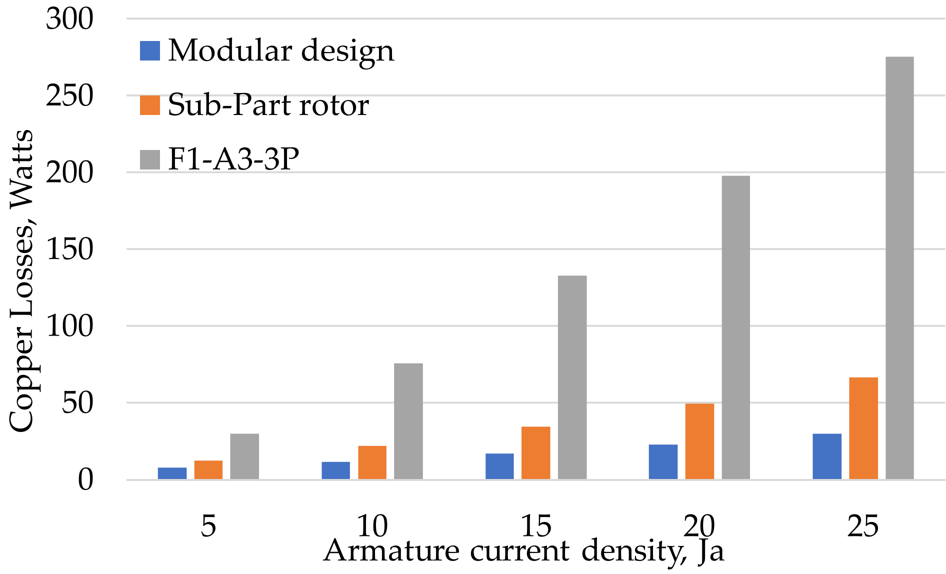

Figure 25. Copper losses versus various J_A

4.12. Iron Loss Versus Speed

Iron loss is a significant portion in the total losses of machine. Machine performance is greatly affected by iron losses due to flux emphasis of novel-modular topology in the stator, which generates variation of flux densities in the rotor and stator core [17, 18]. The flux density variation is expected to reduce by implementing the novel-modular topology due to the reduction in utilization of stator. Iron losses are increased with increasing electrical loading due to higher armature reaction [19]. The iron losses of switched flux machine also greatly varying with speed as shown in Figure 26. At low-speed, machine dominates over electromagnetic losses. The method of iron loss calculation can be found in [17, 20].

The iron loss of each component of three field excited FSM is calculated by 3D-FEA. In Figure 26. the plot clearly shows that the proposed modular rotor structure has lowest iron loss then the conventional sub-part rotor design and F1-A3-3P design. At maximum speed of 4000 rpm, modular design reduces the iron losses of 29.44% and 7.22% compared with the conventional F1-A3-3P design and sub-part rotor design respectively. The reason of iron loss reduction in the stator due to modular rotor, and variation of flux densities in the stator-core is investigated in [21].

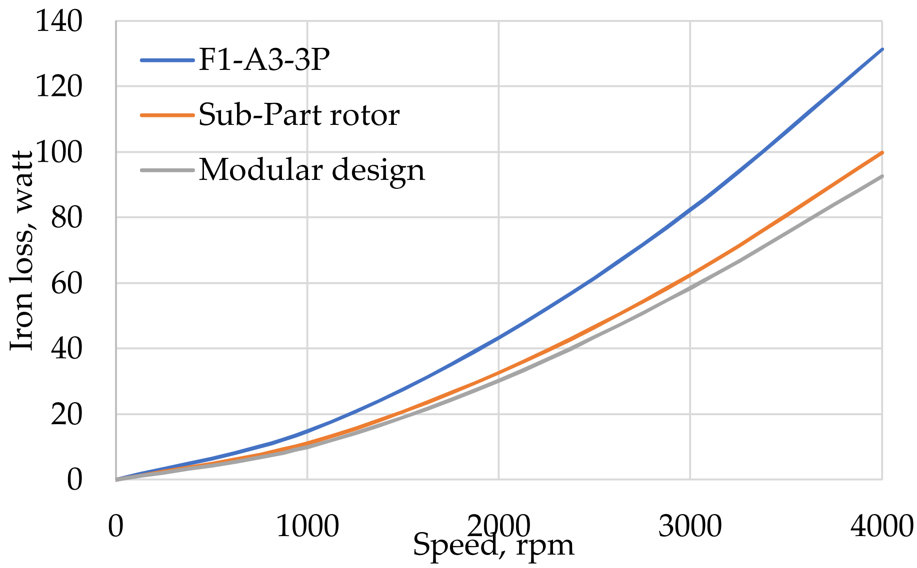

Figure 26. Comparison of iron losses at various speed

Preprints (www.preprints.org) | NOT PEER-REVIEWED | Posted: 18 December 2018 doi:10.20944/preprints201812.0208.v1

Peer-reviewed version available at Energies 2019, 12, 1576; doi:10.3390/en12081576

4.13. Motor Losses And Efficiency Analysis

The efficiency of three FEFSM is computed by 3D-FEA, considering all motor losses (iron losses in core laminations and copper losses in FEC and armature coil). Copper losses(Pcu) is calculated at fixed current densities of 10A/mm², for both FEC, Je, and armature coil, Ja, for all designs. Whilst, the iron losses is calculated at varying speed of 1000-4000rpm. In single phase FEFS machine copper losses can be illustrated as

$$P_{cu} = I_f^2 R_f + I_a^2 R_a \tag{10}$$

Where Pcu, I_f, R_f, I_a and R_a are copper losses, field current, total field coil resistance, armature current and total armature coil resistance, respectively. Figure 27 (a)(b)(c) shows iron losses(Pi) , copper losses(Pcu), output power(Po) and efficiency at different speed(range: 1000-4000rpm) of Sub-part rotor design, F1-A3-3P design and modular rotor design respectively. However, with increasing speed the iron losses is increases as well that further degrade efficiency. Furthermore, at every operating speed from 1000rpm to 4000rpm, the proposed design achieve comparatively higher efficiencies. At max speed of 4000rpm, the iron losses of proposed modular rotor design is 9% and 30% lower than the conventional sub-part rotor design and F1-A3-3P design respectively. However, reduction in iron losses shows a significant reduction in total machine losses, approximately 49% of F1-A3-3P design and 15% of sub-part rotor design. Furthermore, by adopting the modular structure the proposed 8S/6P design achieves higher average efficiency of approximately 12.8% and 11.4% higher than the conventional F1-A3-3P and sub-part rotor design, respectively. Finally, it can be seen from Figure 28, the efficiency of single phase modular 8S/4P FEFS machine exhibit higher efficiency than other conventional FEFS machines.

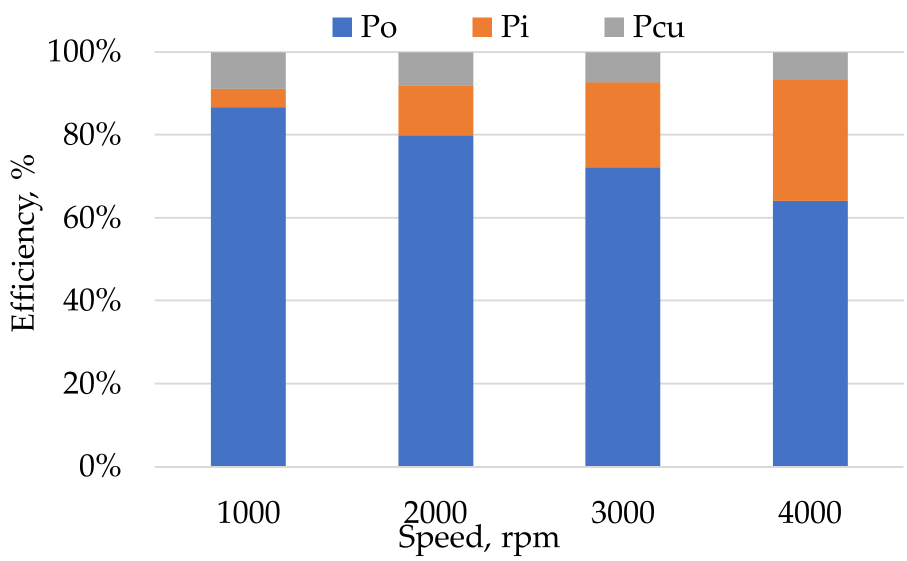

Figure 27(a). Losses and efficiency of sub-part rotor design at various speed.

Preprints (www.preprints.org) | NOT PEER-REVIEWED | Posted: 18 December 2018 doi:10.20944/preprints201812.0208.v1

Peer-reviewed version available at Energies 2019, 12, 1576; doi:10.3390/en12081576

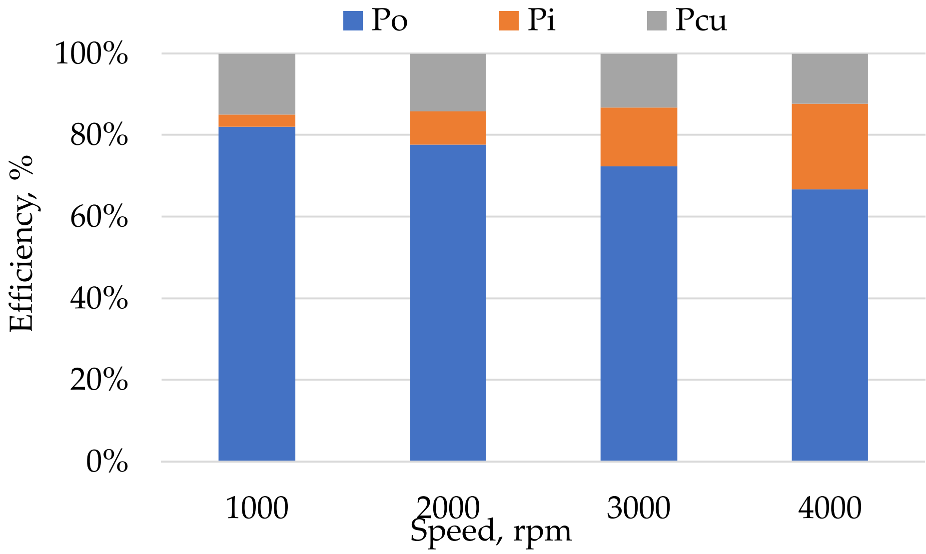

Figure 27(b). Losses and efficiency of F1-A3-3P design at various speed.

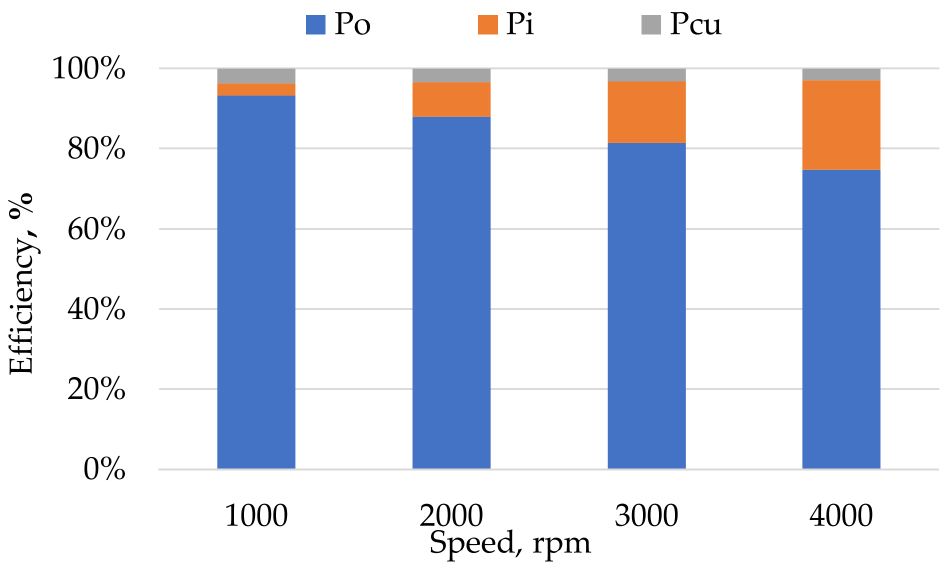

Figure 27(c). Losses and efficiency of modular rotor design at various speed.

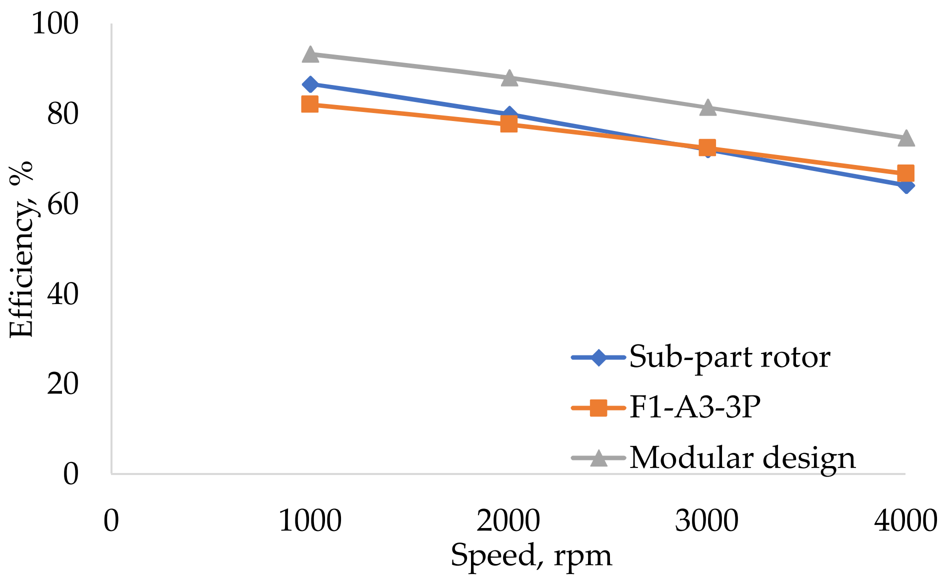

Figure 28. Comparison of efficiency at various rotor speed.

Peer-reviewed version available at *Energies* **2019**, *12*, 1576; doi:10.3390/en12081576

5. Conclusion

A novel single phase field excited topology of modular rotor flux switching machine is presented and the result is validated by 3D-FEA.

In this paper comparison of three single-phase 8-slots/4-pole sub rotor design and 6-slots/3-poles salient rotor design with novel modular rotor 8-slots/6-poles FSM is demonstrated. For pair comparison of flux linkage, cogging torque, average torque and other different analysis of proposed FEFSM, optimal split ratio is set identical to the conventional designs.

Proposed novel modular 8S/6P single phase FSM with non-overlapped winding arrangement is designed. Copper consumption of modular rotor design is much lower than conventional designs due to non-overlap winding between FEC and armature coil. The proposed design shows a higher average output torque when compared under constraints of fixed copper losses. Modular rotor structure also exhibits a significant reduction in iron losses. Due to the modular structure of rotor, the active rotor mass of the proposed design is reduced and lower the use of stator back-iron without diminishing in output torque. This paper also examines the principal rotor stress of the conventional rotor designs (sup-part rotor design and 3-pole salient rotor design) and proposed (modular) rotor design with a different direction of constraints. Additionally, modular rotor design has higher average efficiency as compare to conventional designs, due to considerable reduction in copper losses as well as iron losses.

References

1. You, Zih-Cing, Sheng-Ming Yang, Chung-Wen Yu, Yi-Hsun Lee, and Shih-Chin Yang. "Design of a High Starting Torque Single-Phase DC-Excited Flux Switching Machine." IEEE Transactions on Industrial Electronics, 2017, vol 64, pp. 9905-9913.
2. Khan, Faisal, Erwan Sulaiman, and Md Zarafi Ahmad. "A novel wound field flux switching machine with salient pole rotor and nonoverlapping windings." Turkish Journal of Electrical Engineering & Computer Sciences, 2017, vol 25, pp. 950-964.
3. Omar, M. F., E. Sulaiman, M. Jenal, R. Kumar, and R. N. Firdaus. "Magnetic Flux Analysis of a New Field-Excitation Flux Switching Motor Using Segmental Rotor." IEEE Transactions on Magnetics 2017,vol 53, pp. 1-4.
4. Zhu, Z. Q., and J. T. Chen. "Advanced flux-switching permanent magnet brushless machines." IEEE Transactions on Magnetics 2010,vol 46, pp. 1447-1453.
5. Sangdehi, SM Kazemi, S. E. Abdollahi, and S. A. Gholamian. "A segmented rotor hybrid excited flux switching machine for electric vehicle application." In Power Electronics, Drive Systems & Technologies Conference PEDSTC, 2017, pp. 347-352.
6. Sanabria-Walter, C., H. Polinder, J. A. Ferreira, P. Jänker, and M. Hofmann. "Torque enhanced flux-switching PM machine for aerospace applications." In Electrical Machines ICEM, 2012, pp. 2585-2595.
7. Chen, Yu, Z. Q. Zhu, and David Howe. "Three-dimensional lumped-parameter magnetic circuit analysis of single-phase flux-switching permanent-magnet motor." IEEE Transactions on Industry Applications 2008, vol 44, pp. 1701-1710.
8. Rauch, S. E., and L. J. Johnson. "Design principles of flux-switch alternators." Transactions of the American Institute of Electrical Engineers Power Apparatus and Systems, 1955,vol 74, pp. 1261-1268.
9. Pollock, H., C. Pollock, R. T. Walter, and B. V. Gorti. "Low cost, high power density, flux switching machines and drives for power tools." In Industry Applications Conference, 2003, vol. 3, pp. 1451-1457.
10. Pollock, C., H. Pollock, and M. Brackley. "Electronically controlled flux switching motors: A comparison with an induction motor driving an axial fan." In Industrial Electronics Society IECON, 2003, vol. 3, pp. 2465-2470.
11. Zhou, Y. J., and Z. Q. Zhu. "Comparison of low-cost single-phase wound-field switched-flux machines." IEEE Transactions on Industry Applications, 2014, vol 50, pp. 3335-3345.
12. Pang, Y., Z. Q. Zhu, D. Howe, S. Iwasaki, R. Deodhar, and A. Pride. "Investigation of iron loss in flux-switching PM machines, *4th IET International Conference on Power Electronics, Machines and Drives (PEMD)*, 2008, pp. 460-464.
13. Zhang, Zongsheng, Xu Tang, Daohan Wang, Yubo Yang, and Xiuhe Wang. "Novel Rotor Design for Single-Phase Flux Switching Motor." IEEE Transactions on Energy Conversion, 2018, vol 33, pp. 354-361

14. Zulu, Ackim, Barrie C. Mecrow, and Matthew Armstrong. "A wound-field three-phase flux-switching synchronous motor with all excitation sources on the stator." IEEE transactions on industry applications 2010, vol 46, , pp. 2363-2371.
15. Zhu, Li, S. Z. Jiang, Z. Q. Zhu, and C. C. Chan. "Analytical methods for minimizing cogging torque in permanent-magnet machines." IEEE transactions on magnetics, 2009, vol 45, pp. 2023-2031.
16. Abdollahi, Seyed Ehsan, and Sadegh Vaez-Zadeh. "Reducing cogging torque in flux switching motors with segmented rotor." IEEE Transactions on Magnetics 2013, vol 49, pp. 5304-5309.
17. Pang, Y., Z. Q. Zhu, D. Howe, S. Iwasaki, R. Deodhar, and A. Pride. "Investigation of iron loss in flux-switching PM machines." 2008, pp. 460-464.
18. Hoang, Emmanuel, Mohamed Gabsi, Michel Lécrivain, and Bernard Multon. "Influence of magnetic losses on maximum power limits of synchronous permanent magnet drives in flux-weakening mode." In Industry Applications Conference, 2000. Conference Record of the 2000 IEEE, vol. 1, pp. 299-303.
19. Chen, J. T., Z. Q. Zhu, S. Iwasaki, and R. Deodhar. "Comparison of losses and efficiency in alternate flux-switching permanent magnet machines." In Electrical Machines (ICEM), 2010 XIX International Conference on, IEEE 2010, pp. 1-6.
20. Calverley, Stuart David, G. W. Jewell, and R. J. Saunders. Design of a high speed switched reluctance machine for automotive turbo-generator applications. No. 1999-01-2933. SAE Technical Paper.
21. Thomas, A. S., Z. Q. Zhu, and L. J. Wu. "Novel modular-rotor switched-flux permanent magnet machines." IEEE Transactions on Industry Applications 48, 2012, vol no. 6, pp. 2249-2258.